ACADEMIA ROMÂNĂ
Revue Roumaine de Chimie
https://www.icf.ro/rrch/

Rev. Roum. Chim.,
2023, *68*(3–4), 153–164
DOI: 10.33224/rrch.2023.68.3-4.05

Dedicated to Dr. Maria Zaharescu
on the occasion of her 85th anniversary

PREPARATION AND CHARACTERIZATION OF BIOMIMETIC HETEROGENEOUS CATALYSTS WITH Cu(II) AND Mn(III) COMPLEXES

Mihaela MUREŞEANU,[a] Viorica PARVULESCU,[b,*] Gabriela PETCU,[b] Silviu NASTASE,[c]
Traian D. PASATOIU[c] and Marius ANDRUH[c,d]

[a] University of Craiova, Calea Bucuresti 107I, Craiova, Roumania
[b] "Ilie Murgulescu" Institute of Physical Chemistry of the Roumanian Academy,
Spl. Independentei 202, Bucharest, Roumania
[c] University of Bucharest, Faculty of Chemistry, Bd. Elisabeta nr. 4-12, Bucharest, Roumania
[d] "Costin D. Nenitescu" Institute of Organic and Supramolecular Chemistry of the Roumanian Academy,
Spl. Independentei 202 B, Bucharest, Roumania

Received November 23, 2022

New catalysts were synthesized by immobilization of Cu(II) and Mn(III) biomimetic complexes onto mesoporous SBA-15 silica, amino-functionalized SBA-15, montmorillonite and Al-pillared montmorillonite supports. [Cu(acac)(phen)(OH_2)](ClO_4) and [Cu(acac)(Me_2bipy)](ClO_4) copper complexes and [Mn(III)(valen)(H_2O)(CH_3CN)](ClO_4)·CH_3CN manganese complex supported on silica pore surface or intercalated into the interlayer spaces of clays, were characterized by X-ray diffraction, N_2 adsorption-desorption, TGA-DTA analysis, IR and UV-Vis spectroscopy. These results have confirmed the structural stability of the mesoporous hosts and successful anchoring of the metal complexes over the supports. In order to verify the biomimetic comportment, catalytic activities of the free and immobilized complexes and that of Trametes versicolor laccase, immobilized on the same supports, were tested by oxidation with air of 2,2′-azino-bis(3-ethylbenzothiazoline-6-sulfonic acid), the most used substrate for estimation of specific activity of laccases. The supported complexes were more active than the free ones. Furthermore, the stability tests for the most active heterogeneous catalyst confirmed that the best support was NH_2-SBA-15.

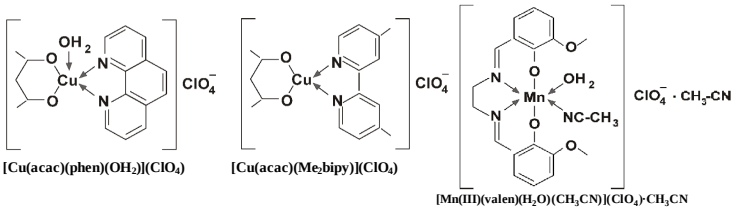

INTRODUCTION

Development of new catalytic systems by immobilization of the homogeneous catalysts on a support is one of the main objectives of the recent research in the field[1]. Such catalysts combine the high selectivity of a homogeneous catalyst and minimize many of the barriers associated with the unremovable homogeneous catalysts. Furthermore it is possible to tune the catalyst reactivity by the choice of supports with different immobilization characteristics[2–4]. The use of transition metal complexes with different biomimetic ligands have been successfully used as models for enzymes in different reaction types, such as the selective oxidation of alkanes, alkenes and aromatic alcohols[5].

* Corresponding author: vpirvulescu@icf.ro

Initially, the complexes were just ion-exchanged or adsorbed on the porous supports and, consequently, could be susceptible to leaching[6–9]. More recently, several grafting and tethering procedures have been developed to covalently attach transition-metal complexes to organic polymers[10–12], silica[13], zeolites[14] and other micro- and mesoporous inorganic materials[15–19]. As a result of the site isolation of transition metal complexes into the support, any bimolecular reaction leading to an oxidative destruction is prevented. Ordered mesoporous solids with their well-defined and highly accessible uniform mesopores and facile surface modification, are potential materials for heterogenization of valuable homogeneous catalysts[20–23]. SBA-15 appears to be one of the best candidates for catalytic support or adsorbent applications due to its regular pore size, a large surface area, a large number of surface silanol groups, and a high chemical and thermal stability[24–26]. Functionalized alkoxysilanes, such as 3-aminopropyltriethoxysilane, allow the subsequent bounding of the catalytic active species. Recently, Cu(II), Co(II) and Fe(III) tetrahydro-salen and chiral [Mn(III)salen] complexes have been successfully immobilized through aminosilane linkers and were applied for catalytic reactions[27,28]. Reports on the heterogenisation of manganese(III) complexes catalysts have been centered on their covalent binding to organic polymers[29] and on their encapsulation, entrapment, adsorption and covalent attachment to porous inorganic supports, such as zeolites, silica, MCM-41, Al-MCM-41, SBA-15 and clays[5,28,30–32], and also on activated carbon[33].

Since many years, pillared cationic clays (PILCs) are potentially important as catalyst support and sorption medium because of their high surface area and porosity[34]. For example, chiral [Mn(III)salen] complexes were encapsulated into aluminium pillared clays and used as heterogeneous catalysts in the epoxidation of styrene[21]. These materials can be prepared from natural expandable clays (such as montmorillonites) and comparatively with cationic clays, posses a 2-dimensional porous network. Smectite clays such as montmorillonite have attracted interest as supports for heterogenised homogeneous catalysts, because they combine cation exchange, intercalation and swelling properties which endows them with the ability to immobilize into their interlayer various cationic species or complexes[35–37]. Montmorillonite is a 2:1 layered aluminosilicate with general formula $M_x(Al_{2-y}Mg_y)Si_4O_{10}(OH)_2 \cdot nH_2O$. Al and Mg atoms are present in octahedral sites forming the central layer of each clay sheet, Si atoms in tetrahedral sites form two layers on either side of the octahedral layer. The sheets have a permanent negative charge resulting from isomorphic substitutions occurring mainly in the octahedral layer. The charge is balanced by counter ions intercalated between the sheets[35]. Properties like swelling and ion exchange nature of the montmorillonite, with gallery heights of around 0.7 nm[36], added the advantage for easy intercalation of guest metal complexes.

Biomimetic properties of copper and manganese complexes are known. In this respect, manganese complexes with various synthetic ligands, *i.e.* Schiff bases, 2, 2'-bipyridine or cyclic triamines are known to be active homogeneous catalysts in the oxidation of olefins and phenols[23] and copper complexes have become a matter of current interest because of their wide applications as catalysts in oxidation of cyclic, aliphatic or aromatic compounds[38–40]. Thus, mono- and binuclear Cu(II) complexes have been investigated as biomimetic catalysts for catechol oxidatio[38,41–43]. Copper complexes with 1,10-phenantroline; 4,4'-dimethyl-2,2'-bispyridyl; acetylacetonate anion have been successfully used in the synthesis of some homo- and heteropolymetallic systems exhibiting interesting optical or magnetic properties[44–47] but until now their catalytic properties have not been studied.

In this paper, we present the synthesis of two Cu(II) biomimetic complexes $[Cu(acac)(phen)(H_2O)](ClO_4)$ and $[Cu(acac)(Me_2bipy)](ClO_4)$ and a Mn(III) complex $[Mn(III)(valen)(H_2O)(CH_3CN)](ClO_4)\cdot CH_3CN$, where acac = acetylacetonate, phen = 1,10-phenantroline, bipy = 2, 2'-bipyridine and valen is a ligand obtained from the condensation of 3-methoxysalicylaldehyde and ethylenediamine (2:1 molar ratio), immobilized onto different supports: non-functionalized and amino-functionalized SBA-15 mesoporous silica, montmorillonite and Al-pillared montmorillonite. The heterogeneous catalysts obtained by immobilization of two Cu(II) and one Mn(III) complexes (Scheme 1) were used as catalysts for the oxidation reaction of 2,2′-azino-bis(3-ethylbenzothiazoline-6-sulfonic acid) = ABTS with air. The biomimetic behavior of the immobilized copper complexes was evidenced by comparing their oxidative catalytic activity with that of the *Trametes versicolor* laccase immobilized in the same supports. In a previous paper[48] we have studied the same enzyme that was immobilized on SBA-15 and amino-functionalized SBA-15 mesoporous silica supports and tested for oxidative degradation of aromatic hydrocarbons. For the measurements of the specific activity of free and immobilized laccase, one of the most common substrate, ABTS, was used. This is why we chose it for the catalytic activity measurements and to prove the biomimetic comportment of the

immobilized cooper and manganese complexes. Furthermore, by correlating the material characterization results with those of catalytic activity and stability tests, the most performant catalytic system for oxidation reactions was proposed.

RESULTS AND DISCUSSION

Two copper (II) complexes (C1, C2) with mixed ligands and the manganese(III) complex (C3) with a Schiff-base ligand previously synthesized were subsequently immobilized on SBA-15, amino-modified SBA-15 and montmorillonite (MM) and Al-pillared montmorillonite (MMA) clay supports from alcoholic solution. As previously reported[49], the average number of silanol groups (quantified by ^{28}Si NMR spectroscopy) for the SBA-15 material is 3.6 OH nm^{-2}. Based on this density of silanol groups, the calculated yield of the aminopropyl grafting was about 86%. The X-ray diffraction (XRD) measurements confirmed typically SBA-15 hexagonal structure for both unmodified and grafted samples by the presence of the strong (100) and the smaller (110), (200) and (210) diffraction peaks[50,51]. There were no significant changes upon amine immobilization, but only the decrease in XRD peak intensity pointed out the functionalization mainly inside the mesoporous channels (Fig.1A).

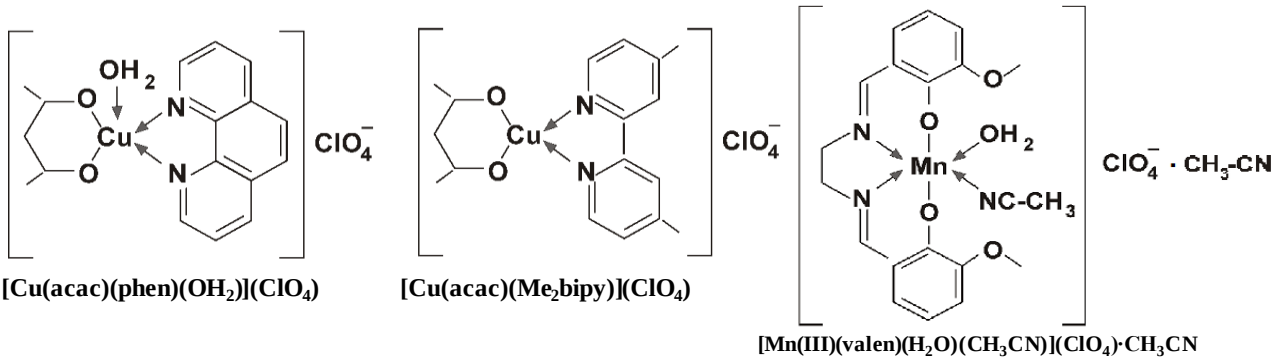

Scheme 1 – Structure of Cu(II) and Mn(III) complexes.

Upon complex immobilization in the functionalized silica framework, a diminuation of the intensity of the main diffraction peak was observed in the XRD patterns, confirming that the short-range hexagonal order was preserved. Crystals of [Cu(acac)(phen)(H_2O)](ClO_4), named C1, have a structure with pentacoordinated Cu(II) ions, containing the acetylacetonate ligand and a 1,10-phenantroline ligand in the basal plane of the pyramid, and a water molecule coordinated in the apical position. The [Cu(acac)(Me_2bipy)](ClO_4) complex, named C2, contains a square-planar Cu(II) ion, the two chelatic ligands – acetylacetonate and Me_2bipy – being almost coplanar. Perchlorate anions are not coordinated. The diffraction pattern (Fig. 1B) reveals that the montmorillonite support exhibited a low intensity reflection peak at 2θ = 5.9º corresponding to d_{001} basal spacing of 1.54 nm. Other characteristic reflections were observed at 2θ = 19.8º, 35º, 55º and 62º. The peaks marked as M are indicative of a 2:1 swelling clay and confirm the characteristics of this type of material. Peaks corresponding to quartz impurity were also indexed. The immobilized [Mn(III)(valen)(H_2O)(CH_3CN)](ClO_4)·CH_3CN, named C3, has structural characteristics almost identical to the montmorillonite support and only a small shift to higher d_{001} value of 1.62 nm was found, confirming the slight swelling in the interlayer of the montmorillonite and the manganese complex adsorption mainly on the silicate and aluminate groups presented at the montmorillonite surface. The similarity between the diffractograms of the materials, indicate that the clay structure is retained during immobilization of the complex. This situation was previously mentioned for other Mn(III) complexes immobilized between the clay layers of montmorillonite[44,52]. The Al-pillared montmorillonite support present d_{001} values of 1.69 nm at 2θ = 5.3º, typical for this type of materials. The diffraction peaks located at 2θ =19.9º, 20.9º, 35.8º and 61.9º could be indexed to a pillared montmorillonite, too. The powder X-ray diffraction pattern of the C3 immobilized into AMM did not have any significant differences from that of parent Al-pillared montmorillonite, apart from a slight higher d_{001} value. This indicates that the pillared structure was retained even after loading of the Mn(III) complex, with a slightly higher layer distance of 1.79 nm.

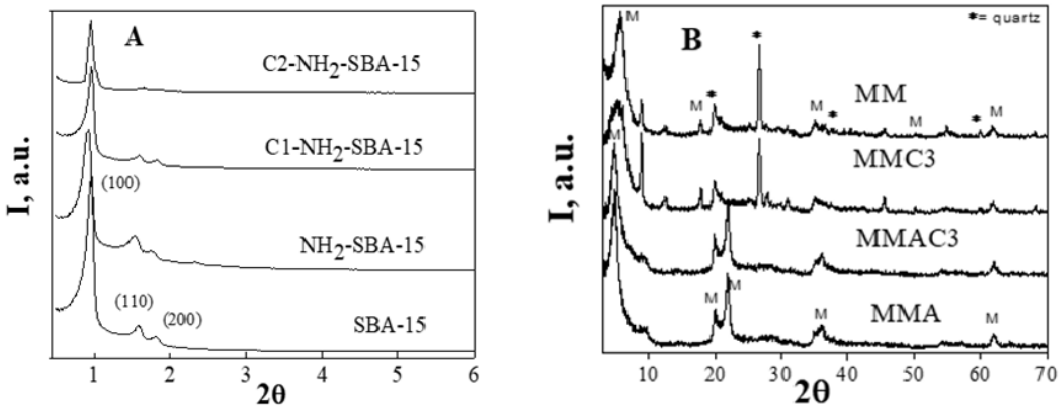

Fig. 1 – XRD- patterns of SBA-15 supports before and after functionalization and immobilization of Cu(II) complexes (A) and of montmorilonite supports before and after immobilization of Mn(III) complexes (B).

Laccases (p-diphenol: dioxygen oxidoreductase, E.C. 1.10.3.2) are multi-copper oxidase having Type 1, Type 2, and Type 3 copper sites. Laccases reduce oxygen directly to water in four-electron transfer step without intermediate formation of soluble hydrogen peroxide in expense of one-electron oxidation of a variety of substrates, e.g., phenolic compounds. *Trametes versicolor* laccase is a globular proteine having 5×5×7 nm dimensions and a molecular weight of 60 kDa. These dimensions allow the enzyme accommodation into micro- and mesopores with diameters higher than 10 nm. *Trametes versicolor* laccase was immobilized by adsorption into SBA-15 or amino-functionalized SBA-15 mesoporous silica[48] as well as in montmorillonite and Al-pillared montmorillonite clay supports in order to obtain an efficient catalyst for the ABTS substrate oxidation. The oxidative catalytic activities of these ones were compared with those of the immobilized copper and manganese complexes. The textural properties of the heterogeneous catalysts were evaluated from the N_2 adsorption-desorption isotherms at 77 K. In Fig. 2 are presented the isotherms of the most active immobilized complex, namely C1- NH_2-SBA-15, in comparison with those of the SBA-15 and NH_2-SBA-15 supports.

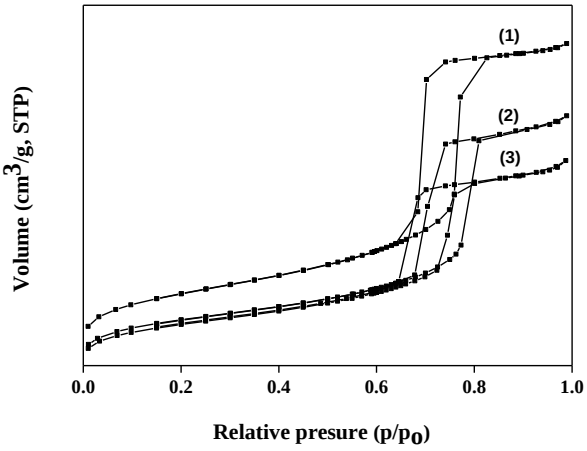

Figure 2. N_2 adsorption-desorption isotherm of : (1) SBA-15, (2) NH_2-SBA-15 and (3) C1-NH_2-SBA-15

The mesoporous silica materials exhibited adsorption-desorption isotherms with a H1 hysteresis loop in the relative pressure range from 0.65 to 0.75, characteristic of materials with 7–8 nm pore diameter. This result reveals that the uniform mesoporous nature of the material is preserved even though the grafting has occurred. The main textural properties of solids are listed in Table 1.

Table 1

Textural properties of calcined and modified SBA-15[a]

Sample	S_{BET} ($m^2\ g^{-1}$)	V_p (mL g^{-1})	d_p (nm)
SBA-15	697.23	1.49	8.23
C1-SBA-15	683.58	1.42	8.15
C2-SBA-15	654.3	1.36	7.83
C3-SBA-15	649.23	1.34	7.80
NH_2-SBA-15	367.75	0.77	7.83
C1-NH_2-SBA-15	316.73	0.73	6.85
C2-NH_2-SBA-15	325.24	0.74	7.12
C3-NH_2-SBA-15	304.25	0.69	6.46

[a]S_{BET} – specific surface area; V_p – pore volume; d_p – pore diameter.

We note that for the functionalized SBA-15 materials, the BET surface area and volume were standardized *versus* pure silica weights. As expected, the BET surface area and the mesopore volume strongly decreased after grafting. For example, for the aminopropyl functionalized mesoporous silica (NH_2-SBA-15) the BET surface area and the mesopore volume were diminished by 53% and 52%, respectively, comparatively to the SBA-15 support. These textural results confirm that the grafted species are located inside the mesopores and not only on the outer surface. No change in the isotherm profile was observed upon complex immobilization, suggesting that the functionalized SBA-15 structure was unaffected by complex anchoring. However, a further decrease in the material surface area and a slight decrease in the mean mesoporore size are observed, confirming indirectly the presence of the complex within the matrices.

The Fourier-transform infrared (FTIR) spectra of the SBA-15 precursor and organic-inorganic hybrid SBA-15 materials are illustrated in Fig. 3A.

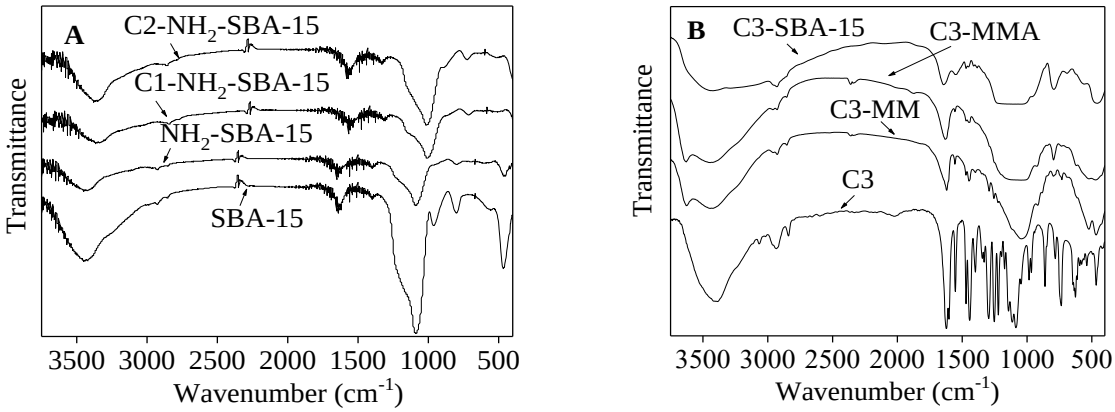

Fig. 3 – FTIR spectra for (A) immobilized copper complexes into SBA-15 type supports and (B) free and immobilized manganese complexes.

The infrared spectrum of the calcined SBA-15 silica shows the typical Si-O lattice vibration: a strong and broad band with two peaks in the 1450–900 cm^{-1} region and two strong bands between 900 and 450 cm^{-1}. Furthermore, a very broad band, centered at 3450 cm^{-1}, attributed to O-H stretching vibrations, can be observed. A band at 1618 cm^{-1} is also observed in the spectrum and it can be assigned to the H-O-H bending vibration of physisorbed water.

Upon amine functionalization, a decrease in the intensity of the bands at 3450 cm^{-1} and at 800 cm^{-1} is observed. Furthermore, the band at 960 cm^{-1} disappeared indicating that reaction of isolated silanol groups of the SBA-15 surface with ethoxy groups of the silane derivative took place. The N-H and C-H stretching vibrations of 3-aminopropyltriethoxysilane (APTES) are observed in the 3400–3000 cm^{-1} region and around 3000 cm^{-1}, respectively, and the corresponding H-N-H and H-C-H bending vibrations can also be observed in the 1700–1500 cm^{-1} and 1500–1300 cm^{-1} spectral regions. The IR spectra of C1-NH_2-SBA-15 and C2-NH_2-SBA-15 show some changes with respect to the parent material in regions where vibration from APTES occur: 3500–3000 cm^{-1} region, due to N-H stretching vibrations and 1700–1300 cm^{-1}, with absorptions due to the H-N-H and H-C-H bending vibrations, suggesting some molecular changes in the spacer. On the other hand, broad bands are observed at 1658 and 1555 cm^{-1}, which may be attributed to a C=N stretching vibration and to acetylacetonate ring vibrations, respectively. C-H stretching vibrations (from phen or dipy rings) appear above 3000 cm^{-1} and characteristic C-H out of plane bending vibrations are seen at 879 and 729 cm^{-1}. These results indicate that there was a Schiff condensation between the free amine groups on the functionalized SBA-15 silica surface and the oxygen atoms coordinated to copper (II), and therefore the complex anchoring on SBA-15 support.

The FTIR spectra of the free manganese complex or immobilized into the clay or silica supports (see Fig. 3B) reveal some characteristic bands of the Mn(III)-Schiff base ligads complexes such as the ν(C=N) vibration at 1622 cm^{-1}, the ν(C=C) vibration of phenyl ring at 1533 cm^{-1}, the ν(C-N) vibration in the range 1398–1331 cm^{-1}, the ν(C-O) vibration at 1295 cm^{-1}. Furthermore, the band at 3386 cm^{-1} could be assigned to N-H stretching vibration of the amide group, the bands between 3000 and 2800 cm^{-1}

due to the C-H stretching vibrations of the Schiff base metoxy groups and the band at 781 cm^{-1} to the ring vibration[53]. There are not significant differences in the IR spectra after C3 heterogenization, confirming its successfully immobilization into the tested supports.

Diffuse reflectance UV-Vis spectroscopy (DR-UV-Vis) was used to characterize the effectiveness of loading of copper species and to observe the nature and coordination state of the copper ions. The DRUV spectra of C1 and C2 complexes immobilized onto SBA-15 silica supports are presented in Fig. 4(A) and were compared with the UV-Vis spectra of the same complexes in alcoholic solutions. The stereochemistry of Cu(II) ions in complexes was evidenced in the UV-Vis spectra by the differences in the bands associated to d-d transitions. [Cu(acac)(phen)(H_2O)](ClO_4) complex, having a CuN_2O_3 chromophore group, gives rise to blue crystals, while [Cu(acac)(Me_2bipy)](ClO_4) is red-brown due to a CuN_2O_2 cromophore[54]. As there were no color changes after complexes immobilization, we can conclude that the stereochemistry of Cu(II) ions in the complexes is the same. Furthermore, DRUV spectra of C1 and C2 anchored SBA-15 catalysts exhibit the same absorption bands as in solution. The intense absorption bands in the UV region (280–330 nm) can be related to the ligands which contain extended π electron systems: π(acac)-π(acac)*, π(phen)-π(phen)*, and π(Me_2bipy)-π(Me_2bipy)* transitions. The absorption bands in the 405–415 nm region could be related to the charge transfer between the ligands and the metallic ions. The bands observed at about 600 nm, for C1-SBA-15 si C2-SBA-15 are due to the d-d transitions of the Cu(II) chromophores. The FTIR and diffuse reflectance UV–Vis spectra of some typical Mn(III)-complex samples are shown in Figs. 3B and 4B, respectively. Clearly, the solid UV–Vis spectra of the three heterogenized Mn(III)–Schiff base complexes (C3-MM, C3-MMA and C3-NH_2-SBA-15), being very similar to that of the homogeneous counterpart, show three strong bands in the 200–450 nm range (see Fig. 4B).

More specifically, the two bands near 233 and 340 nm are assigned to the π-π* transition of the benzene ring of the ligand and the *n*-π* transition of the azomethine chromophore, respectively, while the third band near 400–410 nm is due to metal to ligand charge transfer (MLCT)[55], indicating that the Mn(III)-Schiff-base complex has been successfully immobilized in the tested supports.

Based on the thermogravimetric analysis and spectrometric methods, the amount of metals, complexes and immobilization yield were determined (Table 2, Fig. 5).

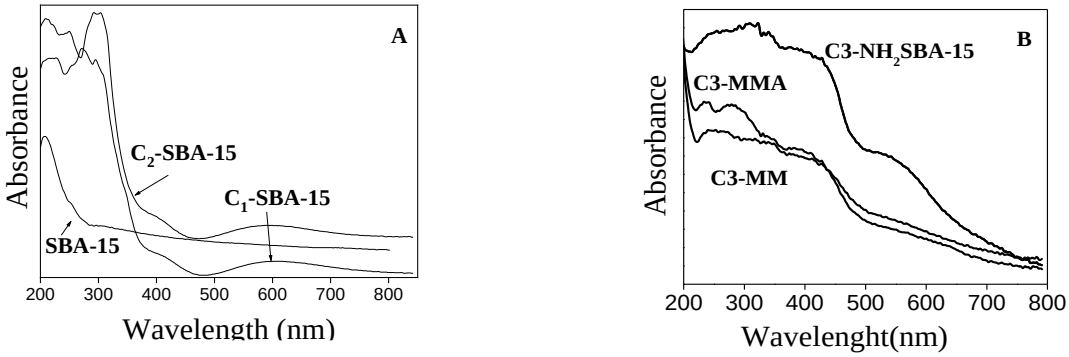

Fig. 4 – DRUV spectra for (A) immobilized Cu(II) complexes and (B) immobilized Mn(III) complex.

Table 2

The metal content and yield of complexes immobilization for different supports

Sample	Cu content (μmol/g)	Mn content (μmol/g)	Metal complexes	
			Spectrometric method (mg/g)	TG/DTA (mg/g)
C1-SBA-15	21.8	–	9.89	10.1
C2-SBA-15	64.07	–	25.67	28.8
C3-SBA-15	–	68.54	30.58	29.32
C1-NH_2-SBA-15	15.06	–	6.24	6.98
C2-NH_2-SBA-15	12.81	–	5.87	5.76
C3-NH_2-SBA-15	–	57.32	22.34	27.76
C1-MM	250.79	–	89.08	93.5
C2-MM	215.73	–	75.56	75.45
C3-MM	–	229.11	103.80	96.44
C1-MMA	234.52	–	82.33	88.40
C2-MMA	163.33	–	55.63	58.70
C3-MMA	–	92.94	44.76	35.98

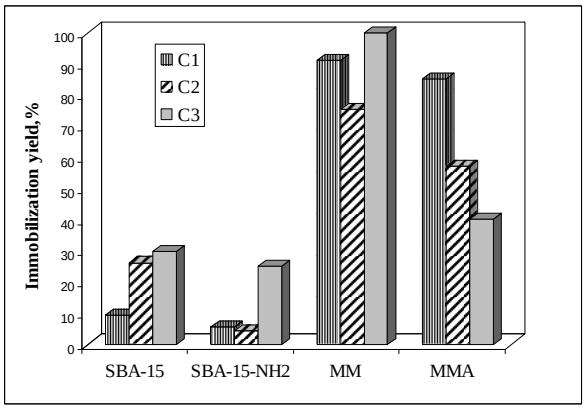

Fig. 5 – Variation of the immobilization yield with support nature and functionalization.

The higher amounts of metals and complexes, as well as the best immobilization yield, were obtained for the montmorillonite support. The higher immobilization yield was obtained for the C3 complex immobilized into montmorillonite clay (100%). Generally, clay type supports presented better immobilization yields comparatively with silica type supports. The pillaring of clay material by alumina modification decreases the amount of immobilization yield of all the complexes, but for the $[Mn(III)(valen)(H_2O)(CH_3CN)](ClO_4)\cdot CH_3CN$ complex there was a more significant decrease. It is important to mention that for the Al-pillared montmorillonite the amount of immobilized complex was smaller for all complexes comparatively with the untreated montmorillonite. Probably, for this last mentioned support, the complexes were immobilized not only by intercallation into the interlamellar space but by adsorption on the external surface, too[55]. Furthermore, the pillars of AMM materials could restrict the complexes intercalation into the interlamelar space.

The obtained results showed a higher influence of the support modification on the amount of the immobilized complexes, probably as a result of surface area decreasing and changing of interaction with the support. Previous publications show that complexes are located inside the pores/voids of SBA-15 and montmorillonite supports[57]. Higher temperature of thermal decomposition of the organics during thermal treatment of supported complexes comparative with free complexes sustains their presence inside the pores of SBA-15 or voids between layers of montmorillonite supports.

The thermogravimetry / differential thermal analysis (TG/DTA) profiles of the heterogeneous complexes biomimetic catalysts (Fig. 6) indicate that immobilization was successful on the tested support materials. The weight loss at temperatures below 473K could be attributed to the loss of adsorbed water. The thermal decomposition of the organic ligand occurred between 523 K and 823 K for C1 and C3 complexes immobilized into different supports, and between 523 K and 723 K, for the immobilized C2 complex, respectively. For the free complexes (C1, C2 and C3) the organic ligand decomposition occurred between 473 K and 1023 K. The obtained results are presented in Table 2.

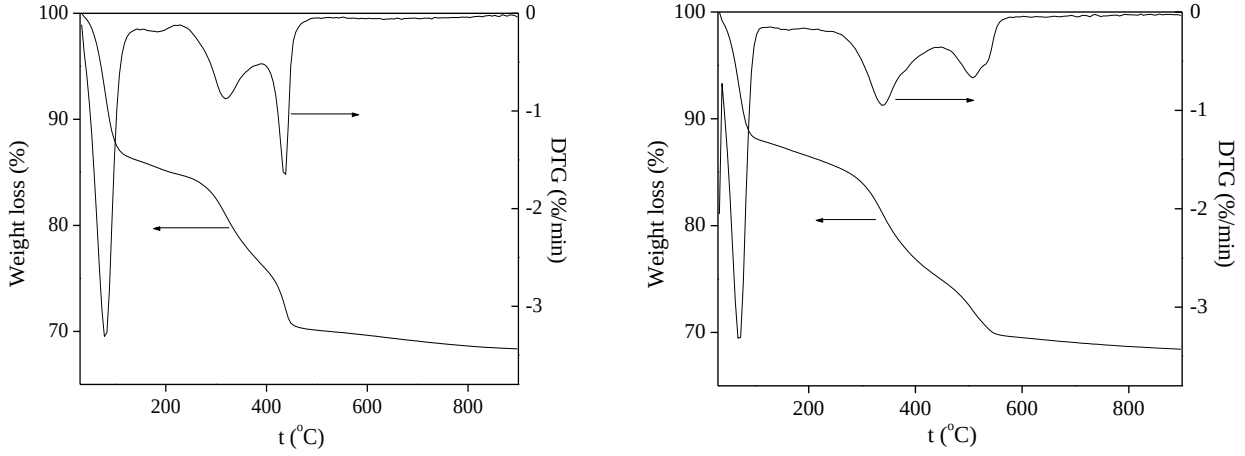

Fig. 6 – TG-DTA curves for: (A) C1 and (B) C2 complexes immobilized into NH_2-SBA-15 support.

For the copper complexes immobilized into different supports, the greatest copper amount was for C1-MM sample (250.79 μmol/g). The order of the immobilization yield was as follows: C1-MM > C1-MMA > C2-MM > C2-MMA > C2-SBA-15 > C1-SBA-15 > C1-NH_2-SBA-15 > C2-NH_2-SBA-15. Comparing the copper complexes immobilized into mesoporous silica, the copper contents was 21.8 μmol/g for C1-SBA-15 sample and 64.07 μmol/g for C2-SBA-15, respectively. Relatively to the copper (II)

complex amounts initially present in each alcoholic solution, the immobilization yields were 9.45% and 26.24% for C1 and C2, respectively. In case of C1 immobilization, the –OH groups present on the surface of SBA-15 silica may have coordinated to the Cu(II) ion, replacing the aqua ligand coordinated in the apical position. For the C2 complex, as there are no water molecules coordinated to the metal ion, only weak interactions between the silica surface and the Cu(II) complex were possible. Consequently, the interactions were less restricted and the amount of immobilized C2 complex was greater than for the C1 complex. Amino-functionalized solids have proved to be less effective in immobilization of complexes. The copper contents were 15.06 μmol/g for C1-NH_2-SBA-15 and 12.81 μmol/g for C2-NH_2-SBA-15 samples and the immobilization yields were 5.77 % for C1, and 4.33 % for C2, respectively.

Considering the BET surface area (Table 1) of the amino-functionalized silica and the molecular surfaces of the immobilized complexes, the maximum estimated capacity of complex immobilization was around 400 μmol/g. Furthermore, the amino groups on the SBA-15 surface are always in great excess relative to the complex. The difference between the theoretical and practical complex content in functionalized SBA-15 materials is probably due to the diffusion control of the metal complex immobilization reaction. Furthermore, as it was proved by the FTIR spectra (Fig. 3A), the complexes immobilization was achieved mainly by the restrictive Schiff condensation between the free amino groups on the surface of the SBA-15 material and the oxygen atoms coordinated to copper (II).

For the manganese Schiff-base complex immobilized into the tested supports, the order of the immobilization yields was the same as for the copper complexes: C3-MM > C3-MMA > C3-SBA-15 > C3-NH_2-SBA-15. In the clay type supports, the manganese amount immobilized into MM was higher (229.11 μmol/g) than the copper amount from C1 and C2 complexes. Contrarily, for the MMA the amount of C3 immobilized was smaller. Probably, the larger manganese complex (L = 7.931Å; l = 12.721 Å, h = 7.835 Å) comparatively with C1 (L = 9.8Å; l = 8.4Å; h ~ 4 Å) and C2 (L = 10.1Å; l = 9.1Å; h ~ 2.5 Å) was slowing down the intercalation into the interlammelar space. The mesoporous silica supports allow a higher immobilization of manganese, comparatively with the copper amounts (68.54 μmol/g for C3-SBA-15 and 57.32 μmol/g for C3-NH_2-SBA-15, respectively). This behavior could be explained by the presence of the metoxy groups on the ligand phenyl ring that allow hydrogen bound with the –OH or –NH_2 groups presented on the silica support surface. On the other hand, the pores diameter is consistent with the C3 complex size.

Trametes versicolor laccase was immobilized by adsorption into different supports. The amount of immobilized enzyme was determined either as equivalent Bovine Serum Albumin (BSA) protein by Bradford method or as organic mass loss from TG-DTA curves (Table 3).

Table 3

The amount and enzymatic activity of immobilized laccase in different supports

Sample	Bradford method (mg/g)	TG/DTA (mg/g)	Yield, %	Activity, (U.I./mg)	Relative activity, %
L-SBA-15	63.00	59.98	40.93	19.90	60.3
L-NH_2-SBA-15	82.33	81.90	67.33	27.75	87.10
L-MM	44.00	49.78	91.29	29.73	90.10
L-MMA	43.09	48.20	88.20	39.04	118.32

When clays were used as support, the immobilization yield and the enzymatic activities were higher than for mesoporous silica supports. Probably, the clay type supports allow an enzyme environment much closer to its natural one. The higher yield obtained for the laccase immobilization into the amino-functionalized SBA-15 silica is probably due to stronger interactions between the enzyme functional groups (-NH_2, -COOH, -OH, -SH) and that of the support surface. For enzyme immobilization the acetone was added to a mixture of the solid support and the buffered enzyme solution in order to produce a forced diffusion of the enzyme into the hydrophilic pores. This method is more efficient than other adsorption methods when much more parameters (such as pH, contact time, temperature, etc.) must be considered. The obtained immobilization yields (Table 3) are similar with those of other research studies on the same type of supports[58].

ABTS oxidation measurements revealed the catalytic activities of the free or immobilized complexes. The initial rate values (calculated from the

concentration of ABTS oxidation product versus time graph) are given in Fig. 7. The calculated initial rate values of the host-free copper complexes (C1 and C2) are about the same (0.48 and 0.50 $\mu M \cdot min^{-1}$). For the manganese C3 complex the initial rate was 1.05 $\mu M \cdot min^{-1}$. The activity of the complexes significantly changed upon immobilization. The most active material towards ABTS oxidation was the $[Cu(acac)(Me_2bipy)]ClO_4$ (C1) complex immobilized into montmorillonite clay support, having nearly 110-fold higher activity than that of the host-free complex. The activity series for immobilized C1 complex was: C1-MM > C1-NH_2-SBA-15 > C1-MMA > C1-SBA-15.

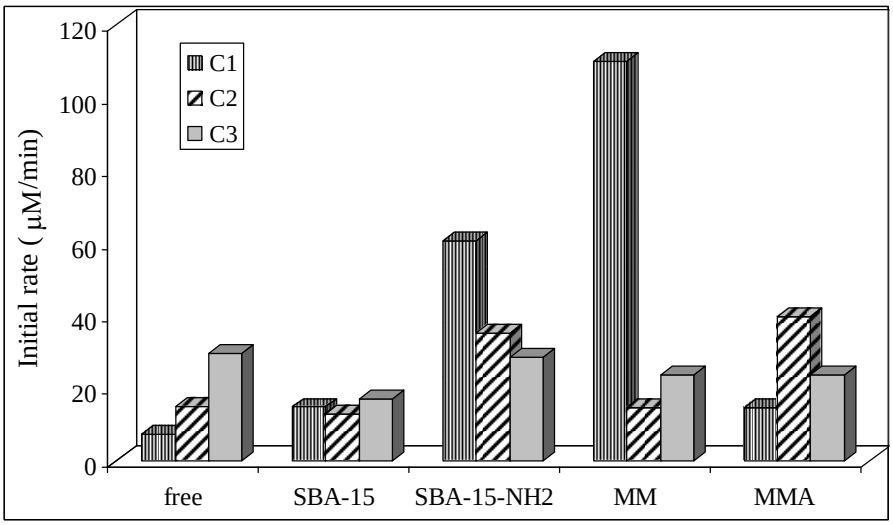

Fig. 7 – Initial rate values of host-free and immobilized copper (II) and manganese (III) complexes in the ABTS oxidation reaction.

Even the C1 amount immobilized into MMA was greater than that immobilized into amino-functionalized silica, the catalytic activity was smaller, confirming the influence of the catalyst environment on its activity. For the immobilized C2 complex, the catalytic activity decreasing as follows: C2-MMA > C2-NH_2-SBA-15 > C2-SBA-15 > C2-MM. In this case, the catalyst activity was not correlated with the amount of immobilized complex but rather with the interactions between complex and support surface that activate the metallic catalyst center. For the NH_2-SBA-15 support, the amount of immobilized complexes was smaller than for the SBA-15. Even so, these catalysts present greater oxidative activities. The initial rate of the ABTS oxidation was higher for both copper complexes after immobilization than for the host-free complexes. This is probably due to additional interactions of the substrate with the support matrix. Thus for C1 and C2 immobilized into NH_2-SBA-15 supports, activities were 60.62 and 39.34 $\mu M \cdot min^{-1}$, respectively with lower activities for the same complexes immobilized into SBA-15 supports.

The immobilized Mn(III)-Schiff-base complex presents the following catalytic activity: C3-NH_2-SBA-15 > C3-MM > C3-SBA-15 > C3-AMM, with activities comparable with those of C2 immobilized complex and that strongly depend on the support surface nature.

In order to evaluate the efficiency of the immobilized copper complexes as biomimetic catalysts, laccase from *T. versicolor* immobilized in the same solid supports was tested also in the ABTS oxidation reaction. The activity of free laccase towards ABTS oxidation with air was firstly determined (33.3 U/mg). The enzymatic activity and the relative activity of the immobilized laccase are given in Table 3. The obtained values suggest that the immobilized laccase posses a much higher oxidative catalytic activity (about 10^3 times) than the biomimetic catalysts. Furthermore, the laccase activity strongly depends on the support surface nature. The greatest relative enzymatic activity was obtained for the laccase immobilized by intercalation into the interlamellar space of the Al-montmorillonite and was correlated with the greatest protein immobilization yield and the best environment that protect the enzyme. The amino-functionalized silica allowed the immobilization of a greater amount of protein, and consequently the enzymatic activity was higher. Unlike complexes, a decrease of the enzymatic activity was evidenced upon enzyme

immobilization. This behavior can be attributed to the more difficult diffusion of the substrate to the active sites of the enzymes due to their tertiary structure. In this study, the enzyme was immobilized in the same supports as the cooper and manganese complexes only for comparing their biomimetic activity. Consequently, further studies will be done for morphological, textural and structural characterization of the heterogeneous catalysts based on laccase and clay supports in order to develop a performant bio catalytic system.

For the purpose of selection the best heterogeneous biomimetic oxidation catalyst we have tested the stability of the catalyst and the metal leaching in five consecutive cycle of use for the C1 complex immobilized into NH_2-SBA-15 and montmorillonite, as these two catalysts presented the greatest activities in the reaction of ABTS oxidation with air. The results of catalyst reusability are presented in Table 4. Surprisingly, even if the catalyst with better activity was the one in which the C1 complex was immobilized in montmorillonite, it lost 40% of its catalytic activity after the first cycle of use, following that after five cycles, its activity was 66% lower compared to the initial one. For the C1-NH_2-SBA-15 catalyst, the loss of activity in the firs cycle was of only 0.23% and after the fifth cycle of 10%. In both cases, the reduction of the catalytic activity can be correlated with the copper leaching in the solution. Additional studies are needed to stabilize the complexes in the lamellar structure of montmorillonite. Taking in account all these considerations the best biomimetic catalyst for the tested oxidation reaction was C1-NH_2-SBA-15 catalyst and consequently, NH_2-SBA-15 was the best support for metallic complexes immobilization.

Table 4

Reusability of C1 complex immobilized in two different support

No. of cycles	Catalytic activity as initial rate of oxidation of ABTS with air (μM/min)	
	C1-NH_2-SBA-15	C1-MM
1	60.48	65.4
2	58.31	58.21
3	56.89	47.26
4	55.43	42.84
5	54.56	37.25

EXPERIMENTAL

1. Synthesis of catalysts

1.1. Preparation of Cu (II) and Mn(III) complexes and their immobilization

Crystals of [Cu(acac)(phen)(H_2O)](ClO_4), named C1, and [Cu(acac)(Me_2bipy)](ClO_4), named C2, were obtained through slow evaporation of the solvent at room temperature (η = 80–85 %). The synthesis of the mononuclear Cu (II) complexes is based on the reaction of an aqueous solution containing 2 mmols of $Cu(ClO_4)_2$ to which are simultaneously added an ethanolic solution containing 2 mmols of neutral chelatic ligand (phen, bipy, Me_2bipy) and an aqueous solution containing 2 mmols of acetyl acetone previously deprotonated with LiOH[52–55]. Crystals of [Cu(acac)(phen)(H_2O)](ClO_4) (denoted C1) and [Cu(acac)(Me_2bipy)](ClO_4) (denoted C2) were obtained through slow evaporation of the solvent at room temperature (η = 80–85%). Selected IR data (KBr, cm^{-1}): C1 – 3440, 3070, 3031, 2983, 1586, 1517, 1427, 1383, 1322, 1272, 1252, 1221, 1142, 1115, 1086, 1020, 924, 856, 786, 764, 723, 682, 626; C2 – 3063, 2362, 1617, 1565, 1524, 1420, 1372, 1282, 1100, 1027, 926, 842, 797, 620.

The [Mn(III)(valen)(H_2O)(CH_3CN)](ClO_4)·CH_3CN (denoted C3) was synthesized following a step by step approach. First, the tetradentate Schiff base H_2valen was prepared by refluxing 3-methoxysalicylaldehyde and ethylenediamine (2:1 molar ratio) in methanol. Then, 10 mL acetonitrile solution containing 0.77 g $Mn(ClO_4)_2·6H_2O$ (2.1 mmol) was added dropwise, under stirring, to a solution obtained by the dissolution of 0.69 g (2.1 mmol) of the tetradentate Schiff base H_2valen in 30 mL acetonitrile. After 3h of continuous stirring at ambient temperature, the resulted brown mixture was filtered. The slow evaporation of the filtrate yielded black-reddish crystals of C3. The crystal structure was confirmed by single-crystal X-ray diffraction[55]. Selected IR data (KBr, cm^{-1}): 3376, 3069, 3016, 2978, 2945, 2844, 1622, 1603, 1553, 1470, 1444, 1398, 1344, 1332, 1302, 1256, 1222, 1173, 1120, 1086, 984, 967, 863, 847, 780, 734, 646, 625, 638.

0.1 g of copper or manganese complexes in 10 mL methanol were slowly added to 1 g of SBA-1 or NH_2-SBA-15 silica support, prepared by previously described procedures[45,46], in 20 mL methanol. The resultant mixture was refluxed for 24 h, filtered, washed with solvent and dried under vacuum at room temperature. The same procedure was used for the complexes immobilization into the clay supports: commercially available montmorillonite-MM (untreated, Fluka) and aluminum pillared montmorillonite-MMA (surface area 250 m^2/g, pH 4–5, Fluka).

1.2. Immobilization of laccase into mesoporous silica and clay supports

Laccase from *T. versicolor* (Sigma) with an activity of 34 I.U. mg^{-1} protein was used without further purification. Immobilization of laccase was carried out by physical

adsorption. In a typical procedure, 1 g support (SBA-15, SBA-15-NH_2, MM or MMA) was mixed with 10 mL of 0.1 M phosphate buffer (pH = 7.0) in a centrifuge tube. Thereafter, 50 mg laccase in 3 mL phosphate buffer were added to the mixture and homogenized under magnetic stirring at 278 K. In this suspension acetone (30 mL) was added drop wise and the stirring was continued for another 30 minutes. The solid was isolated by centrifugation, washed and dried using lyophilizer and stored at 253 K, in dark.

The protein content in immobilized supports was estimated by determining the protein from the supernatant liquid by Bradford assay[56]. The amounts of immobilized laccase were evaluated from the TG/DTA curves and compared with the results of the Bradford assay. The immobilization yield was determined as the ratio between the amount of immobilized protein and the initial protein amount.

2. Characterization

The copper and manganese contents of all samples were determined by flame atomic absorption spectroscopy (FAA) after their dissolution in 10% HF. The immobilization yield was calculated either from the TG/DTA analysis or as a difference between the complex concentrations of the initial and filtrate solutions, determined by UV-Vis spectrometry. Small-angle XRD data were acquired on a Bruker diffractometer using Cu Kα radiation. N_2 adsorption–desorption isotherms were measured at 77 K with a Micromeritics ASAP 2010 instrument. The samples were previously degassed under vacuum at 323 K for 12 h. FTIR spectra of all samples were performed in KBr pellets using a Bruker Alpha spectrometer. FAAS measurements were performed on a Spectra AA-220 Varian spectrometer equipped with Varian multi-element hollow cathode lamps and air-acetylene burner. The UV-Vis spectra were recorded using a Thermo Scientific (Evolution 600) spectrometer. UV-Vis-NIR diffuse reflectance spectra were measured with Lambda 14 spectrometer (Perkin-Elmer Inc., Shelton, USA) with an integrating sphere (Labsphere, North Sutton, USA) for solid samples. Thermogravimetric analysis was carried out in a Netzsch TG 209C thermobalance, by heating the samples up to 850ºC, with a heating rate of 10ºC/min, in an N_2 atmosphere.

3. Activity measurements

Catalytic activities of the host free and immobilized complexes were tested by oxidation with air of 2,2′-azino-bis(3-ethylbenzothiazoline-6-sulfonic acid) (ABTS). The ABTS oxidation reaction in the presence of host-free complexes was monitorized in the same maner as for the free laccase. In order to make initial rates and conversions comparable, the reaction mixture always contained the same amount of Cu(II) or Mn(III). The results were evaluated from the absorption band of ABTS oxidation product at 424 nm and 296 K, using a Cu(II) or Mn(III): ABTS ratio of 1:42. The pH value was kept at 4.5 with acetate buffer and the solution was saturated in oxygen by air bubbling before the starting of the catalytic test. In such conditions, an enzyme solution of one unit/mL (U.I./mL) was required to oxidize 1 μmol ABTS per minute. For the C1 complex immobilized into SBA-15-NH_2 and MM, the reusability of the heterogeneous catalyst was tested in five consecutive runs of ABTS oxidation with air. After each cycle, the recovered catalyst was dried and analyzed for the copper content by FAAS technique in order to evaluate the metal leaching during the catalytic tests.

For the determination of immobilized laccase activity, 10 mg of active solids were added to 50 mL of 1mM ABTS in 0.1 M acetate buffer (pH = 4.5), which was allowed to circulate through the spectrophotometric cell theromostated at 296 K. The enzymatic activity was expressed in U.I./mg of immobilized protein or as relative activity:

$$\text{E.A.\%} = \frac{U^{solid}/\text{mg}}{U^{solution}/\text{mg}} \times 100.$$

CONCLUSIONS

New biomimetic catalysts were obtained by immobilization of two copper, [Cu(acac)(phen)(H_2O)]ClO_4 and [Cu(acac)(Me_2bipy)]ClO_4, and one manganese, [Mn(III)(valen)(H_2O)(CH_3CN)](ClO_4)·CH_3CN complexes on SBA-15, NH_2-functionalized mesoporous silica or montmorillonite and Al-pillared montmorillonite supports. The successful anchoring of the catalysts over the supports and the structural integrity of the host materials were confirmed by various characterization techniques. The oxidation activities of complexes after immobilization have been proved to be higher than in the homogeneous phase. In order to sustain the biomimetic comportment of the heterogeneous catalysts, *Trametes versicolor* laccase was immobilized into the same supports and their catalytic activity tested in the same reaction of ABTS substrate oxidation. Furtherore, the stability tests for the most performant [Cu(acac)(phen)(H_2O)]ClO_4 complex immobilized into different supports confirmed that SBA-15-NH_2 support was the best choice for catalyst heterogenization.

REFERENCES

1. M. J. Alcón, A. Corma, Marta Iglesias and F. Sánchez, *J. Organomet. Chem*., **2002**, *655*, 134–145.
2. D. E. De Vos, B. F. Sels and P. A. Jacobs, *Adv. Catal*., **2001**, *46*, 1–87.
3. M. G. Russell, C. Veryser, J. F. Hunter, R. L. Beingessner and T. F. Jamison, *Adv. Synth. Catal*., **2020**, *362*, 314–319.
4. A. E. Fernandes, A. M. Jonas and O. Riant, *Tetrahedron*, **2014**, *70*, 1709–1731.
5. P. Ratnasamy and D. Srinivasa, *Catal. Today*, **2009**, *141*, 3–11.
6. N. E. Leadbeater and M. Marco, *Chem. Rev*., **2002**, *102*, 3217–3273.
7. J. S. Rafelt and J. H. Clark, *Catal. Today*, **2000**, *57*, 33–44.
8. J. Nakazawa and Y. D. Shiro Hikich, *Mol. Catal*., **2017**, *443*, 14–24.
9. S. Liu, W. Xu, W. Liu, L. Li and J. Wang, *Catal. Today*, **2021**, *382*. 13–21.
10. Q.-H. Fan, Y.-M. Li and A. S. C. Chan, *Chem. Rev*., **2002**, *102*, 3385–3466.

11. T. Maharana, N. Nath, H. C. Pradhan, S. M. . Routaray and A. Kumar Sutar, *React. Funct. Polym*., **2022**, *171*, 105142.
12. P. C. Selvaraj and V. Mahadevan, *Inorg. Chem. Commun*., **2020**, *122*, 108230.
13. S. Uruş, *Appl. Surf. Sci*., **2022**, *593*, 153398.
14. B. Kumar Kundu, V. Chhabra, N. Malviya, R. Ganguly, G. S. Mishra and S. Mukhopadhyay, *Microporous Mesoporous Mat*., **2018**, *271*, 100–117.
15. D. Brunel, N. Belloq, P. Sutra, A. Cauvel, M. Laspéras, P. Moreau, F. Di Renzo, A. Galarneau and F. Fajula, *Coord. Chem. Rev*., **1998**, *1085*, 178–180.
16. R. Hu, L. Zha and M. Cai, *Catal. Commun*., **2010**, *11*, 563–566.
17. S. Yılmaz, E. Genç Acar, G.Yanalak, E. Aslan, M. Kılıç, İ. H. Patır and Ö. Metin, *Applied Clay Science*, **2021**, *205*, 106064.
18. M. Asgari, G. Vitale and U. Sundararaj, *Mol. Catal*., **2022**, *525*, 112365**.**
19. J. Xu, Y. Hong, M.-J. Cheng, B. Xue and Y.-X. Li, *Microporous Mesoporous Mat*., **2019**, *285*, 223–230.
20. P. Das, I. Kuźniarska-Biernacka, A.R. Silva, A.P. Carvalho, J. Pires and C. Freire, *J. Mol. Catal. A: Chem*., **2006**, *248*, 135–143.
21. H. M. Hultman, M. de Lang, M. Nowotny, I. W. C. E. Arends, U. Hanefeld, R. A. Sheldon and T. Maschmeyer, *J. Catal*., **2003**, *217*, 264–274.
22. M. E. Davis, *Nature*, **2002**, *417*, 813–821.
23. D. Trong On, D. Desplantier-Giscard, C. Danumah and S. Kaliaguine, *Appl. Catal. A*, **2003**, *253*, 545–602.
24. M. Tada, R. Coquet, J. Yoshida, M. Kinoshita and Y. Iwasawa, *Angew. Chem. Int. Ed*., **2007**, *46*, 7220–7223.
25. K. Feng, R. Y. Zhang, L. Z. Wu, B. Tu, M. L. Peng, L. P. Zhang, D. Zhao and C. H. Tung, J. *Am. Chem. Soc*., **2006**, *128*, 14685–14690.
26. J. V. Nguyen and C. W. Jones, *Macromolecules*, **2004**, *37*, 1190–1203.
27. Y. Yang, Y. Zhang, S. Hao and Q. Kan, *Chem. Eng. J*., **2011**, *171*, 1356–1366.
28. L.-L. Lou, S. Jiang, K. Yu, Z. Gu, R. Ji, Y. Dong and S. Liu, *Micropor. Mesopor. Mater*., **2011**, *142*, 214–220.
29. M. R. Maurya and J. C. Pessoa, *J. Organomet. Chem*., **2011**, *696*, 244–254.
30. S. M. G. Pires, R. De Paula, M. M. Q. Simões, M. Graça P. M. S. Neves, I. C. M. S. Santos, A. C. Tomé and J. A. S. Cavaleiro, *Catal. Commun*., **2009**, *11*, 24–28.
31. R. I. Kureshy, I. Ahmad, N. H. Khan, S. H. R. Abdi, K. Pathak and R. V. Jasra, *J. Catal*., **2006**, *238*, 134–141.
32. B. Bahramian, V. Mirkhani, M. Moghadam and S. Tangestanineja, *Catal. Commun*., **2006**, *7*, 289–296.
33. A. R. Silva, V. Budarin, J. H. Clark, B. de Castro and C. Freire, *Carbon*, **2005**, *43*, 2096–2105.
34. T. J. Pinnavaia, *Science*, **1983**, *220*, 365–371.
35. A. Cadene, S. Durand-Vidal, P. Turq, J. Brendle and J. Colloid *Interface Sci*., **2005**, *285*, 719–730.
36. N. Khaorapapong and M. Ogawa, *Appl. Clay Sci*., **2007**, *35*, 31–38.
37. S. Tanase and E. Bouwman, *Adv. Inorg. Chem*., **2006**, *58*, 29–75.
38. A. L. Abuhijleh, *Inorg. Chem. Commun*., **2011**, *14*, 759–762.
39. S. Rayati, S. Zakavi, M. Koliae, A. Wojtczak and A. Kozakiewicz, *Inorg. Chem. Commun*., **2010**, *13*, 203–207.
40. K. C. Gupta and A. K. Sutar, *J. Mol. Catal. A: Chem*., **2008**, *280*, 173–185.
41. D. Zois, C. Vartzouma, Y. Deligiannakis, N. Hadjiliadis, L. Casella, E. Monzani and M. Louloudi, *J. Mol. Catal. A: Chem*., **2007**, *261*, 306–317.
42. J. Kaizer, J. Papp, G. Speier, L. Parkanyi, L. Korecz and A. Rockenbauer, *J. Inorg. Biochem*., **2002**, *91*, 190–198.
43. M. C. Mimmi, M. Gullotti, L. Santagostini, A. Saladino, L. Casella, E. Monzani and R. Pagliarin, *J. Mol. Catal. A: Chem*., **2003**, *204-205*, 381–389.
44. R. Palkovits, C. M. Yang, S. Olejnik and F. Schüth, *J. Catal*., **2006**, *243*, 93–98.
45. M. Mureseanu, V. Parvulescu, R. Ene, N. Cioatera, T. D. Pasatoiu and M. Andruh, *J. Mater. Sci*., **2009**, *44*, 6795–6804.
46. M. Filip, G. Petcu E.M. Anghel, S. Petrescu, B. Trica, P. Osiceanu, N. Stanica, I. Atkinson, C. Munteanu, M. Mureseanu and V. Parvulescu, *Catal. Today*, **2021**, *366*, 10–19.
47. A. M. Madalan, V. Ch. Kravtsov, D. Pajic, K. Zadro, Y. A. Simonov, N. Stanica, L. Ouahab, J. Lipkowski and M. Andruh, *Inorg. Chim. Acta*, **2004**, *357*, 4151–4164.
48. M. Mureseanu, I. Trandafir, C. Babeanu, V. Parvulescu and G. Paun, *Environ. Prot. Eng*., **2016**, *42*, 81–95.
49. A. M. Madalan, C. Ruiz-Pérez, E. Melnic, V. Ch. Kravtsov and M. Andruh, *Rev. Roum. Chim*., **2005**, *50*, 11–17.
50. A. M. Madalan, M. Noltemeyer, M. Neculai, H. W. Roesky, M. Schmidtmann, A. Müller, Y. Journaux and M. Andruh, *Inorg. Chim. Acta*, **2006**, *359*, 459–467.
51. T. D. Pasatoiu, A. M. Madalan and M. Andruh, *Rev. Roum. Chim*., **2010**, *55*, 947.
52. M. M. Bradford, *Anal. Biochem*., **1976**, *72*, 248–254.
53. K. Mitra, S. Biswas, C. R. Lucas and B. Adhikary, *Inorg. Chim. Acta*, **2006**, *359*, 1997–2003.
54. R. I. Kureshy, I. Ahmad, N. H. Khan, S. H. R. Abdi, K. Pathak and R. V. Jasra, *J. Catal*., **2006**, *238*, 134–141.
55. Z. Fu, H. Liao, D. Xiong, Z. Zhang, Y. Jiang and D. Yin, *Microporous Mesoporous Mater*., **2007**, *106*, 298–303.
56. R. Margalef-Català, P. Salagre, E. Fernández and C. Claver, *Catal. Lett*., **1999**, *60*, 121–123.
57. V. Ramaswamy, M. Sivarama Krishnan and A.V. Ramaswamy, *J. Mol. Catal. A: Chem*., **2002**, *181*, 81–89.
58. X. Hu, X. Zhao and H.-M. Hwang, *Chemosphere*, **2007**, *66*, 1618–1626.